Journal of Cellular Biochemistry

HSP-enriched properties of extracellular vesicles involve survival of metastatic oral cancer cells

Journal:	*Journal of Cellular Biochemistry*
Manuscript ID	JCB-17-1174.R1
Wiley - Manuscript type:	Research Article
Date Submitted by the Author:	29-Mar-2018
Complete List of Authors:	Ono, Kisho; Okayama University Graduate School of Medicine, Dentistry and Pharmaceutical Sciences Eguchi, Takanori; Okayama University Graduate School of Medicine, Dentistry and Pharmaceutical Sciences, Sogawa, Chiharu; Okayama University Graduate School of Medicine, Dentistry and Pharmaceutical Sciences Calderwood, Stuart; harvard, Futagawa, Junya; Mitsui Knowledge Industry Kasai, Tomonari; Okayama Daigaku, Department of Medical Bioengineering, Graduate School of Natural Science and Technology Seno, Masaharu; Okayama Daigaku, Department of Medical Bioengineering, Graduate School of Natural Science and Technology Okamoto, Kuniaki; Okayama University Graduate School of Medicine, Dentistry and Pharmaceutical Sciences Sasaki, Akira; Okayama University Graduate School of Medicine, Dentistry and Pharmaceutical Sciences, Department of Oral and Maxillofacial Surgery Kozaki, Ken-ichi; Okayama University Graduate School of Medicine, Dentistry and Pharmaceutical Sciences
Keywords:	extracellular vesicle, heat shock proteins, lymph-node-metastatic oral cancer, EV proteomics, exosome, molecular chaperone

HSP-enriched properties of extracellular vesicles involve survival of metastatic oral cancer cells

Kisho Ono[1,2], Takanori Eguchi[1,3,*], Chiharu Sogawa[1], Stuart K Calderwood[4], Junya Futagawa[5], Tomonari Kasai[6], Masaharu Seno[6], Kuniaki Okamoto[1], Akira Sasaki[2] and Ken-ichi Kozaki[1]

1 Department of Dental Pharmacology,

2 Department of Oral and Craniofacial Surgery,

3 Advanced Research Center for Oral and Craniofacial Sciences,

Graduate School of Medicine, Dentistry and Pharmaceutical Sciences / Dental School, Okayama University, Okayama, 700-8525, Japan.

4 Department of Radiation Oncology, Beth Israel Deaconess Medical Center, Harvard Medical School, Boston, MA, USA.

5 Biomedical Department, Solution Center, Mitsui Knowledge Industry, Tokyo, 105-6215, Japan.

6 Department of Medical Bioengineering, Graduate School of Natural Science and Technology, Okayama University, Okayama, 700-8530, Japan.

*Correspondence should be addressed to:

Takanori Eguchi, DDS, PhD

2-5-1, Shikata-cho, Kita-ku, Okayama city, 700-8525, Japan

Phone: +81-86-235-6662

Fax: +81-86-235-6664

E-mail: eguchi@okayama-u.ac.jp

Running title: HSP-enriched vesicles of metastatic cancer

Keywords: extracellular vesicle, heat shock proteins, lymph-node-metastatic oral cancer, EV proteomics, exosome, molecular chaperone

Number of figures: 6

Number of table: 2

Number of supplemental items: 4

Number of references: 47

Word count (Introduction to Discussion): 5442 words

FUNDING. This work was supported by JSPS KAKENHI, grant numbers JP16K11722 (to JM and TE), JP17K11642 (to TE) and JP17K11669 (to KO, CS, and TE) and a Ryobi Teien Memorial Foundation Grant (to TE). Mitsui Knowledge Industry Co., Ltd. provided support in the form of salaries for JF, but did not have any additional role in the study design, data collection and analysis, decision to publish, or preparation of the manuscript.

Abbreviations: EV, extracellular vesicle; HNC, head and neck cancer; HSP, heat shock protein; MV, microvesicle; OSCC, oral squamous cell carcinoma.

Abstract (< 150 words)

Cancer cells often secrete extracellular vesicles (EVs) that carry heat shock proteins (HSPs) with roles in tumor progression. Oral squamous cell carcinoma (OSCC) belongs to head and neck cancers (HNC) whose lymph-node-metastases often lead to poor prognosis. We have examined the EV proteome of OSCC cells and found abundant secretion of HSP90-enriched EVs in lymph-node-metastatic OSCC cells. Double knockdown of HSP90α and HSP90β, using small interfering RNA significantly reduced the survival of the metastatic OSCC cells, although single knockdown of each HSP90 was ineffective. Elevated expression of these HSP90 family members was found to correlate with poor prognosis of HNC cases. Thus, elevated HSP90 levels in secreted vesicles are potential prognostic biomarkers and therapeutic targets in metastatic OSCC.

INTRODUCTION

Oral squamous cell carcinoma (OSCC) accounts for approximately 3% of all human malignancies and for 24% of all head and neck cancers (HNCs) and is trending upward yearly [Jemal et al., 2011]. Regardless of recent advancements in many therapeutic strategies, OSCC remains associated with recurrence and progression. More than 50% of OSCC patients exhibit lymph node metastasis, one of the most common adverse prognostic factors in OSCC patients [Kowalski and Sanabria, 2007; Sano and Myers, 2007]. The 5-year survival rate of primary OSCC patients is greater than 80% but it falls to 40% with cervical lymph node metastasis and falls to 20% with distant metastases [Neveille and Day, 2002]. Cancer progression is often associated with extracellular molecules released by cancer cells into the milieu [Stivarou and Patsavoudi, 2015]. Such secreted molecules can educate cells in autocrine, paracrine and/or endocrine manners, thus inducing changes in tumoral, stromal, endothelial, immune/inflammatory, and distant cells. Extracellular vesicles (EVs) are surrounded by lipid bilayer membranes and contain a variety of cargos such as proteins, nucleic acids, lipid, and minerals [Colombo et al., 2014; Fujita et al., 2016; Pan et al., 1985; Skog et al., 2008]. It has been shown that cargos of EVs can be often transported to recipient cells where they exert their functions [Valadi et al., 2007]. According to vesicle size, EVs are classified as exosomes (30 to 200 nm), microvesicles (MVs) (100 to 1,000 nm), apoptotic bodies (1,000 to 5,000 nm), and matrix vesicles (found in extracellular matrices and carrying abundant minerals) [Lotvall et al., 2014; Raposo and Stoorvogel, 2013; Shapiro et al., 2015; Witwer et al., 2013]. EVs, in particular exosomes usually contain tetraspanins including CD9 [Andreu and Yanez-Mo, 2014] and cancer exosomes

often contain epithelial cell adhesion molecule (EpCAM) [Madhavan et al., 2015; Munz et al., 2009]. We showed highly surviving cancer stem-like cells to robustly secrete EpCAM-contained EVs [Eguchi et al., 2018b]. It was also shown that levels of epidermal growth factor (EGFR) were elevated in serum EVs as well as primary tumors in patients suffering from head and neck squamous cell carcinoma [Overmiller et al., 2017]. Notably, HSP90 was also found in EVs secreted by cancer cells [Clayton et al., 2005; Eguchi et al., 2018b].

HSP family members are molecular chaperones that bind loosely to *de novo* translated proteins or structurally unfolded proteins and promote folding or refolding of proteins that acquire physiological functions or induce proteasomal or lysosomal degradation of proteins [Murshid et al., 2013]. It has been reported that HSPs are overexpressed in various cancer tissues, correlating with disease incidence, progression and lymph node metastasis rate [Ciocca and Calderwood, 2005; Ciocca et al., 1993; Eguchi et al., 2018a; Gong et al., 2015]. The HSP family is composed of subfamilies including HSP70 family, HSP90 family, small HSP family (HSP27 family, HSPB family), and large HSP family (HSP105 / HSP110 family). Among these subfamilies, HSP90 is one of the major intracellular molecular chaperones and plays a role in interacting with various intracellular proteins to ensure its correct folding and function [Workman et al., 2007]. HSP90 can promote tumor growth and metastasis in breast cancer, leukemia, pancreatic cancer and ovarian cancer [Ciocca et al., 1993; Neckers and Workman, 2012]. HSP90 is composed of a number of proteins including cytoplasmic HSP90α, an inducible type, and HSP90β, a constitutively expressed type as well as mitochondrial TRAP1. Although their

expression levels increase under stressed condition and in cancer cells, HSP90β is one of the most abundant proteins in the cytoplasm of unstressed cells. HSP90 proteins act in an ATP-dependent manner as essential factors for the client protein to function properly in the cytoplasm in response to signals, in cooperation with co-chaperones including CDC37 [Calderwood, 2015]. Many of the proteins folded by HSP90-CDC37 complexes are involved in cell growth, and the HSP90-CDC37 complex is an attractive candidate for cancer chemotherapy [Calderwood, 2015; Neckers and Workman, 2012]. In addition to their intracellular roles, HSP-contained EVs and EV-free HSPs have been also found in the extracellular space [Clayton et al., 2005; Eguchi et al., 2018b; Li et al., 2013].

In the present study, we have investigated the EV chaperonome of metastatic OSCC cells, which is involved in cancer cell survival and thus prognosis of OSCCs.

MATERIALS AND METHODS

Cell culture

HSC-3 OSCC cell line and its metastatic subline HSC-3-M3 [Matsui et al., 1988] were obtained from JCRB cell bank at National Institutes of Biomedical Innovation, Health, and Nutrition. For maintenance, these cell lines were cultured in DMEM containing 10% FBS, and the medium was replaced in every 3 days.

Isolation of EVs

We compared the polymer-based precipitation (PBP) method as described [Eguchi et al., 2018b] and the ultracentrifugation (UC) method [Lotvall et al., 2014; Witwer et al., 2013]

to isolate EVs, as shown in a flow chart (Fig. S1A). Cells growing in two 10-cm dishes were washed with Hanks' balanced salt solution (HBSS), and then further cultured in 4 ml of serum-free medium per a dish for 2 days. Cell culture supernatant was centrifuged at 2,000 × *g* for 30 min at 4°C to remove detached cells. The supernatant was then centrifuged at 10,000 × *g* for 30 min at 4°C to remove cell debris. In addition, the supernatant was filtered with a 0.2-μm syringe filter. In the PBP method, the supernatant (8 ml) was concentrated to less than 1 ml by using an Ultra-15 Centrifugal Filter Devices for MW. 100,000 (Amicon). The concentrate was applied to Total Exosome Isolation (ThermoFisher Scientific). The EV fractions were eluted in 100 μl PBS (-). In the UC method, 8 ml of the supernatant was centrifuged at 100,000 × *g* for 70 min (RP-42 rotor, Hitachi). Total EVs pellets were rinsed in PBS (-), centrifuged at 100,000 × *g* for 70 min and suspended in 100 μl of PBS (-). For protein assay, 10 μl of 10 × RIPA buffer containing 10% NP-40, 1% SDS, and 5% deoxycholate in PBS (-) and a EDTA-free protease inhibitor cocktail (Sigma) were added to the 100 μl of the EV fraction and incubated on ice for 30 min. Thirty-five microliter of the EV was used for protein assay using micro BCA protein assay system (ThermoFisher Scientific).

Transmission electron microscopy (TEM)

As described [Eguchi et al., 2018b]. A 400-mesh copper grid coated with formvar / carbon films was hydrophilically treated. The EV suspension (5 to 10 μl) was placed on Parafilm, and the grid was floated on the EV liquid and left for 15 min. The sample was negatively stained with 2% uranyl acetate solution for 2 min. EVs on the grid were visualized with

20,000 times magnification with an H-7650 transmission electron microscope (Hitachi, Tokyo, Japan) at Central Research Laboratory, Okayama University Medical School.

To determine the EV sizes, lengths of the major axes of 50 EVs between 50 nm and 200 nm-diameters in the TEM images were measured. To examine statistical homoscedasticity of those 2 groups, F-test was performed with a null hypothesis that variances of those 2 groups were equal. Paired Student's t-test was then performed.

Particle diameter analysis

Forty µl of EV fraction within PBS (-) was used. Particle diameters of the EV fractions in a range between 0 and 1,000 nano-diameters were analyzed in Zetasizer nano ZSP (Malvern Panalytical, UK).

ExoScreen

ExoScreen was performed as described [Yoshioka et al., 2014]. Serial dilution standards of exosome were prepared from a 50 ng/µl of CD9 positive exosome fraction prepared from HCT116 cells. PBS (-) was used for a negative control. For CD9 positive exosome ExoScreen, 5 µl of EV fraction was mixed with 20 µl of a mixture of acceptor beads immobilized with anti-CD9 antibodies and biotinylated anti-CD9 antibodies in a white 96-well plate. The plate was centrifuged briefly and was shaken with a vortex. The samples were incubated at room temperature (RT) for 1 h with avoiding light. Then, 25 µl of 80 µg/ml streptavidin-immobilized donor beads were added. The plate was centrifuged briefly, and vortex. The samples were incubated at RT for 30 min without light. After

adding excitation light (wave length 680 nm), the light of emission (wave length 615 nm) was measured in EnSpire AlphaLISA system (PerkinElmer). ExoScreen was performed with duplicate per each EV fraction. For analysis of CD9-EpCAM double positive exosome, 5 ng/μl CD9-EpCAM standard protein and its step dilution were used for standard, and acceptor beads immobilized with anti-CD9 antibodies and biotinylated anti-EpCAM antibodies were used. The samples were measured with duplicate in the ExoScreen-AlphaLISA system.

Whole cell lysate

As described [Eguchi et al., 2018b]. Cells cultured on a 10-cm dish were washed with 5 ml of PBS (-) and then collected by using a cell scraper and centrifuged for 5 min at 4 °C at 1,000 × *g*. The cells were washed with PBS (-) and centrifuged again. Then, 1000 μl of a 1 × RIPA buffer containing 1% NP-40, 0.1% SDS, and 0.5% deoxycholate in PBS (-) and protease inhibitors were added to the cellular pellet. Cells were then lysed through a 25-gauge syringe for 10 strokes. The cell lysate was incubated for 30 min on ice and then centrifuged at 15,000 × *g* for 20 min at 4 °C to pellet cell debris. The supernatant was used as a whole cell lysate (WCL). The WCL was diluted 10-fold, and protein concentration was measured by using micro BCA protein assay system (ThermoFisher Scientific).

Western blotting analysis

As described [Eguchi et al., 2018b]. Equal amounts of protein samples in each Western blotting analysis (each 4 μg of protein samples for analysis of CD9, EpCAM, HSP90α and

β-actin, and each 10 μg of protein samples for analysis of EGFR, HSP90β and GAPDH) were separated by SDS-PAGE in in 4-20% TGX-GEL (BioRad) and transferred to PVDF membranes by using a semi-dry method. The membranes were blocked in Tris-buffered saline (TBS) containing 0.05% Tween 20 (TBS-T) and 5% ECL Blocking Agent (GE Healthcare) for 1 h with shaking at RT. Each membrane was incubated overnight with shaking at 4˚C with primary antibodies: either mouse anti-CD9 (1:1,000, MBL), mouse anti-EpCAM (1:1,000, Cell signaling technologies), rabbit anti-HSP90α (1:5,000, GeneTex), rabbit anti-HSP90β (1:1,000, GeneTex), or rabbit anti-EGFR (1:1,000, Abcam). Afterwards, horseradish peroxidase (HRP)-conjugated anti-mouse IgG (1:10,000, cell signaling technologies) or anti-rabbit IgG (1:10,000, GE Healthcare) secondary antibodies were incubated for 1 h with shaking at RT. Washes before and after antibody reactions were done on a shaker, three times within TBS-T for 10 min at RT. Alternatively, membranes were incubated with HRP-conjugated mouse anti-β-actin (1:5,000, Wako) or anti-GAPDH (1:10,000, Wako) antibodies for 1 h with shaking at RT. Blots were visualized with a ECL Plus Western blotting substrate (Pierce).

Mass spectrometry

Liquid chromatography and tandem mass spectrometry (LC-MS/MS) was carried out as described previously [Eguchi et al., 2008]. The EV fractions were used for short SDS-PAGE (approx. 4 mm) in 4-20% TGX-GEL (BioRad) and visualized with Coomassie Brilliant Blue stain (BioRad). Gel fragments containing the stained protein bands were excised, then minced into 1 × 1 to 2 × 2 mm pieces. The proteins were digested by using In-Gel Tryptic

Digestion Kit (ThermoFisher Scientific). The gel pieces were destained with mixture of ammonium bicarbonate and acetonitrile. The protein samples were reduced with 50 mM Tris [2-carboxyethyl] phosphine (TCEP), and alkylated with iodoacetamide (IAA). In order to shrink gel fragments, acetonitrile was added and incubated for 15 min at RT after which the acetonitrile was removed and the gel pieces were air dried for 5-10 min. Ten microliter of MS grade trypsin (Pierce) at concentration of 0.1 mg/ml was added to the air-dried sample and incubated at RT for 15 min. Ammonium bicarbonate at a final conc. of 25 mM was added to the sample, digested overnight at 30 °C, and the extract was recovered. Subsequently, a 1% formic acid solution was added to the gel pieces, incubated for 5 min, and the supernatant was added to the extract. Extracts containing digested peptides were measured by Agilent 6330 Ion Trap LC / MS System with MASCOT database search engine at Central Research Laboratory, Okayama University Medical School. The cutoff score for proteins was 11.0. The score was defined based on the covering rate for amino acid sequences and the frequency of detected fragments. The data of MS were analyzed as described previously by using 2-Dimensional Image-Converted Analysis of LC-MS/MS (2DICAL2) software (Mitsui Knowledge Industry, Tokyo, Japan) [Ono et al., 2012]. The detected protein species were collated with the ExoCarta database [Mathivanan et al., 2012]. Among the protein species detected in the EVs of each cell line, the top 50 protein species were selected with reference to the MS score. Protein species specifically detected in each EV fraction were classified according to their biological function and compared based on the number of protein species or MS score.

Prognostic values of *HSP* genes expression in tumor samples resected from HNC patients

To examine prognostic values of *HSP* gene expression in clinical samples of HNCs, we retrieved The Human Protein Atlas [Uhlen et al., 2015]. HNCs patients (n = 499) were distinguished between high expression group and low expression group in each gene. Correlation between gene expression levels and prognosis of patients were shown as Kaplan-Meier survival analyses. The high- or low-expression group was examined at each stage of HNC (stage 1: n = 25, stage 2: n = 69, stage 3: n = 78, stage 4: n = 259). The ratio (high expression group / low expression group) was calculated for each stage, and the correlation between gene expression level and stage progress of HNC was examined.

RNAi

We designed siRNA species that target each mRNA coding HSP90α, HSP90β, and CDC37 individually (Table S1). The synthesized siRNA was RNA duplex of 19 bp plus TT-3' overhangs in each strand. For targeting each mRNA, a mixture of two types of siRNA were used.

Electroporation-transfection

Electroporation was performed using NEPA21 electroporator (NEPA Gene, Ichikawa, Japan) according to the manufacturer's recommendation. HSC-3-M3 cells (5×10^5 cells) were centrifuged at 1,000 × *g* for 5 min at RT and suspended in 100 μl of serum-free DMEM with 40 pmol siRNA. Poring pulse condition was 250 V, 1.5 milliseconds (ms) pulse

length, total two pulses, 50 ms interval between the pulses, and 10% decay rate with + polarity. The transfer pulse condition was 20 V, 50 ms pulse length, total five pulses, 50 ms interval among the pulses, 40% decay rate with +/- polarity. After the electroporation, cells were immediately suspended into DMEM containing 10% FBS and seeded at concentration of 5×10^5 cells / 2 ml in a well of 6-well plates. Three days after the electroporation, cells were harvested for cell counting and Western blotting.

Cell survival

Cells were transfected with siRNA using electroporation and then seeded as described above. Cells were washed with PBS (-) at 24 hours after the transfection and further cultured in 2 ml of DMEM containing 10% FBS per a well for 2 days. Cells were detached using Trypsin/EDTA at 3 days post-transfection period and number of cells were counted using Countess® Automated Cell Counter (ThermoFisher Scientific). Photomicrographies were taken using Floid® Cell Imaging Station (ThermoFisher Scientific).

Statistical analysis

Statistical significance was calculated using Microsoft Excel. Difference of two sets of data were examined with a paired Student's t-test. $P < 0.05$ was considered to indicate statistical significance. Data were expressed as means ± S.D. unless otherwise specified.

RESULTS

Preparation of EVs using the PBP method and the UC method

Several methods for EV preparation have been established as follows: UC method, PBP [Eguchi et al., 2018b], affinitiy capturing [Nakai et al., 2016], sucrose density gradient, size exclusion chromatography, filtration, immunological separation, isolation by sieving, and their combinations [Lobb et al., 2015; Lotvall et al., 2014; Witwer et al., 2013]. These methods have distinctive mechanism of EV preparation with advantages and disadvantages. We in the present study tested PBP and UC methods for isolation of EVs from culture supernatants of HSC-3 OSCC cell line and its metastatic subline HSC-3-M3 (Fig. S1 A). Particles sized between 50 and 200 nm-diameters with cup-shaped morphology were found in the EV fraction prepared by using the PBP method, suggesting exosomes and/or MVs (Fig. S1 B, upper TEM images). A few EV-like particles were also found in the EV fraction isolated by the UC method (Fig S1 B, lower TEM images). To examine EV collection efficiency, we next measured protein concentration of EVs. The ratio of EV protein concentration per the cellular protein concentration was approximately 3.0% in the PBP method-used EVs whereas it was approximately 1.5% in the UC method-derived EVs, suggesting that EVs were more efficiently collected using the PBP method. We therefore used the PBP method for preparation of EVs in the following studies.

The metastatic OSCC cells secrete larger EVs compared to those secreted by parental OSCC cells.

We prepared EVs from culture supernatants of HSC-3 and HSC-3-M3 cells by using the PBP method shown above and analyzed their morphological difference of EVs under TEM. EVs

with a cup-shaped morphology were found in EV fractions of both HSC-3 and HSC-3-M3 cells, indicating that both cell lines secrete exosomes and/or MVs (Fig. 1 A, B).

It has been shown that the sizes of exosomes are present in a range between 50 and 200 nm-diameters while those of MVs are between 100 and 500 nm [Colombo et al., 2014; Fujita et al., 2016]. To investigate if the OSCC cells secrete exosomes, we next examined the sizes of EVs in the range between 50 and 200 nm secreted by metastatic and parental OSCC cells. Vesicles sized between 50 and 200 nm were found in the EV fractions of both cell types, which were suggested to secrete exosomes. The median and mean of the diameters of HSC-3-M3-derived EVs (109 nm and 111.8 nm, respectively) were significantly larger than those of HSC-3-derived EVs (80.7 nm and 94.6 nm, respectively), indicating that HSC-3-M3 secreted larger EVs than HSC-3 (Fig. 1 C).

To investigate whether these OSCC cells secrete MVs in addition to exosomes, we next analyzed particle diameter distributions of the EVs. Both cell types secreted EVs with single peaks, indicating that these EV fractions had some homogeneity (Fig 1 D, E). The HSC-3-EVs were sized in a range between 50 and 450 nm-diameters whereas the HSC-3-M3-EVs were sized in a range between 50 and 500 nm-diameters, suggesting that the metastatic cells might secrete more MVs (Fig 1 D, E). Consistently, the size peak of HSC-3-EVs was found at 155.1 nm whereas that of HSC-3-M3-EVs was shifted to 167.1 nm (Fig. 1 D, E).

These results indicated that the metastatic OSCC cells secrete larger EVs than those derived from the parental OSCC cells.

Metastatic OSCC cells secrete more EpCAM-EVs than their parental OSCC cells

We next examined levels of CD9, which is generally contained in most exosomes, and EpCAM, which is more often found in cancer exosomes. CD9 and EpCAM were present in HSC-3-M3-EVs at higher levels than in the parental cells-derived EVs (Fig 2A). The elevated levels of EpCAM and CD9 in HSC-3-M3-EVs were found using both PBP and UC methods with similar tendnecies.

We next examined CD9 positive exosomes and CD9-EpCAM double positive EVs using ExoScreen, a sensitive and rapid analytical system with two types of antibodies that capture EVs and detect the presence of exosomes with photosensitizer-beads [Yoshioka et al., 2014]. HSC-3-M3 cells secreted more CD9 positive exosomes than HSC-3 cells: levels of CD9 positive exosomes per EV fraction were and 4.5% (HSC-3) and 8.2% (HSC-3-M3), respectively (Fig. 2B). The CD9 positive exosome concentration was 360 ng per 10^6 cells (HSC-3) and 640 ng per 10^6 cells in HSC-3-M3 (Fig. 2C), consistent with the data from Western blotting shown above.

We next examined the levels of CD9-EpCAM double positive exosomes (v/w % per EV fraction and ng per 10^6 cells) in the two cell lines. HSC-3-M3 cells secreted more CD9-EpCAM double positive exosomes than HSC-3 cells: CD9-EpCAM double positive exosomes per EV fraction were 2.8% (HSC-3) and 3.6% (HSC-3-M3), respectively (Fig. 2D). CD9-EpCAM double positive exosomes (ng) per 10^6 cells was 220 ng per 10^6 cells (HSC-3) and 275 ng per 10^6 cells (HSC-3-M3), respectively (Fig. 2E), consistent with the data from Western blotting shown above.

These results suggested that the EpCAM level in exosomes could be a potential biomarker of lymph-node-metastatic OSCC cells.

The metastatic OSCC cells profoundly secrete HSP90-EVs.

To characterize the metastatic OSCC cells and their EVs, we next examined whether HSP90, EpCAM, EGFR, GAPDH, and β-actin were contained in the EVs that were secreted by HSC-3 and HSC-3-M3. The level of HSP90α was profoundly higher in the HSC-3-M3-EVs and in the HSC-3-M3 cells as compared to those of HSC-3, suggesting that HSP90α increased in this metastatic type of OSCC cells that then abundantly secreted HSP90α-EVs (Fig 3, top). Of note, HSP90β was specifically found in the HSC-3-M3-EVs but not in the HSC-3-EVs while cellular HSP90β was reduced in HSC-3-M3 as compared to the parental cells, suggesting that metastatic OSCC cells can selectively secrete HSP90β-EVs that may be involved in the metastatic phenotype (Fig 3, the second from the top).

We next examined levels of EpCAM and EGFR trans-membrane oncoproteins in the EVs and cells. EpCAM was profoundly at a high level in the HSC-3-M3-EVs as compared to the HSC-3-EVs while cellular EpCAM was reduced in HSC-3-M3 as compared to the parental cells, suggesting that metastatic OSCC cells can actively secrete EpCAM-EVs that may involve metastatic phenotype (Fig 3, the third from the top). Most EGFR appeared to be retained in these OSCC cells, although HSC-3-M3 secreted EGFR-EVs more than HSC-3 cells.

Housekeeping proteins such as GAPDH and β-actin have been also found in EVs [Durcin et al., 2017; Mathivanan and Simpson, 2009]. The levels of GAPDH and β-actin

were not altered between HSC-3-M3 and HSC3 and between their EV fractions, suggesting that these housekeeping proteins may be useful as loading controls in analysis of EVs as well as cell lysates.

These results indicate that metastatic OSCC cells can robustly secrete HSP90-EVs and EpCAM-EVs that may involve their metastatic phenotype. Another inference to be drawn from this data is that the levels of proteins found in the cytoplasm do not necessarily predict their levels in EVs (Fig. 3). Relative levels of Hsp90α and EpCAM are relatively high compared to their intracellular concentrations while the opposite is true for Hsp90β, GAPDH and EGFR (Fig. 3).

A proteome signature of OSCC-EVs

To characterize OSCC cells and their EVs, we next analyzed the EV proteomes of HSC-3-M3 and HSC-3 by mass spectrometry. Within the prepared EV fractions, total 192 protein species were identified commonly between in HSC-3-EVs and HSC-3-M3-EVs (Fig. 4A). To examine whether these EVs contained known and novel EV proteins, we next compared these OSCC-EV proteins with EV proteins registered in the ExoCarta database [Mathivanan et al., 2012]. Among the 192 protein species in the OSCC-EVs, 108 EV protein species (56.3%) were already registered in ExoCarta and 84 EV protein species (43.7%) were not registered yet and thus potentially novel EV proteins (Fig. 4A).

To characterize the metastatic phenotype of OSCC cells associated with their EVs, we next compared the nature of the top 50 EV protein species between the HSC-3-M3-EVs and HSC-3-EVs. Thirty two percentage of the EV protein species was

distinct for each of the cell types, suggesting that these specific proteins could play a role in metastatic phenotype within the two cell lines (Fig. 4B). To further characterize differences in the proteomes, we next classified the top 16 EV protein species according to their known functions. The functioal classification of EV proteins revealed that the HSC-3-M3-EVs carried more molecular chaperones and cytoskeletal proteins, and less extracellular matrix (ECM) proteins than HSC-3-EVs (Fig. 4 C, D).

We next investigated the molecular chaperone species in these OSCC-EVs. Among the total 192 EV protein species, 14 types of molecular chaperones were identified and 9 of them were specifically at high levels in HSC-3-M3-EVs as compared to HSC-3 EVs (Fig. 4E). The MS score ratios for the molecular chaperones (HSC-3-M3 / HSC-3) were 1.78 (HSP90α), 2.23 (HSP90β), 2.95 (TRAP1, mitochondrial HSP90), and 1.78 (HSP105 / HSPH1), respectively (Table 1) (It was confirmed by western blotting analysis that HSP90-enriched EVs were secreted by the metastatic OSCC cells line as shown in Table S2 and Fig 3).

It was thus suggested that lymph-node-metastatic OSCC cells secreted EVs enriched in particular HSPs, which could be thus useful markers for prognosis of OSCC cases.

Prognostic values of *HSP* gene expression in clinical tumor samples of head and neck cancers

As levels of HSPs in EVs likely reflect their relative intracellular expression, we investigated correlation between *HSP* gene expression levels in tumors and prognosis of

patients suffering from HNCs. We examined clinical values of *HSP90AA1* (coding HSP90α), *HSP90AB1* (coding HSP90β), *TRAP1* (coding mitochondrial HSP) and *HSPH1* (coding HSP105) genes by using The Human Protein Atlas [Uhlen et al., 2015]. HNC patients were distinguished between high and low expression groups for each gene and survival rates were compared using Kaplan-Meier analysis. The 5-year survival rate of each chaperone high expression group of *HSP90AA1*, *HSP90AB1*, *TRAP1*, and *HSPH1* was lower than that of each low expression group, respectively (Fig. 5, Table S3), indicating that high expression of these HSPs could be correlated to poor prognosis of HNCs. In particular, the ratio (high expression group / low expression group) valued by *HSP90AA1* expression level in stage 1 (n = 25) of HNCs was 0.39 whereas that in stage 4 (n = 259) was 1.21, indicating that *HSP90AA1* expression could increase along with progression of HNCs (Table 2). The ratio valued by *HSP90AB1* expression level in stage 1 of HNCs was 0.14 whereas that in stage 4 was 0.57 (Table 2). The ratio valued by *TRAP1* expression level in stage 1 of HNCs was 2.57 whereas that in stage 4 was 4.18 (Table 2). Thus, these three genes increased the proportion of the high expression group as the stage of HNC progressed. In contrast, the ratio valued by *HSPH1* expression level in stage 1 of HNCs was 3.17 whereas that in stage 4 was 2.20 (Table 2).

These data suggest that high expression of *HSP90AA1, HSP90AB1,* and *TRAP1* are potentially useful for prognosis of HNC patients. It should be kept in mind in vewing the data that the relationship between intracellular gene expression and secretion in EV can be complex (Fig. 3). However increased intracellular expression of HSPs is likely to lead to greater release in EVs. The relative roles of intracellular and extracellular

chaperones in cancer is currently under assessment and their relative significance still under debate [Calderwood, 2018].

Double knockdown of HSP90α and HSP90β declined survival of metastatic OSCC cells

We next examined whether siRNA-mediated knockdown of HSP90 could alter survival of metastatic OSCC cells. The siRNA targeting of HSP90α lowered the HSP90α level but did not lower survival of HSC-3-M3 cells. The siRNA targeting of HSP90β slightly lowered the HSP90β level as well as survival of HSC-3-M3 cells (Fig. 6). Of note, siRNA double targeting of HSP90α and HSP90β profoundly lowered HSP90β and HSP90α levels and significantly lowered survival of HSC-3-M3 cells as compared to the single knockdown effect (Fig. 6). We next examined involvement of CDC37, a co-chaperone of HSP90 in the cell survival studies. Interestingly, CDC37 level was reduced by knockdown of either HSP90α or HSP90β but not by double knockdown of HSP90α/β, suggesting that this co-chaperone could be destabilized upon reduction in the partner HSP90 but with potentially compensatory mechanism (Fig. 6). Triple knockdown of HSP90α/β and CDC37 also significantly lowered survival of metastatic OSCC cells (Fig. 6).

These findings indicate that the siRNA-mediated double targeting of HSP90α and HSP90β could be a potential therapeutic in metastatic OSCC.

DISCUSSION

Metastatic and parental OSCC cells secreted EVs (Fig 1-3, Fig S1), although their relative sizes (Fig 1), levels of cancer EV markers (Fig 2, 3), EV proteome signatures (Fig 4), and EV chaperone signatures (Fig 3, 4, Table 1) were significantly different between these two types of cancer cells. It has been known that a size range of exosomes can be between approx. 50 and 200 nm-diameters whereas that of MVs can be between approx. 100 and 500 nm [Raposo and Stoorvogel, 2013]. A single cell type such as platelets, endothelial cells, and breast cancer cells releases both exosomes and MVs [Heijnen et al., 1999]. The OSCC cells secreted EVs sized between 50 and 500 nm with a peak at approx. 160 nm, indicating that these EV fractions included exosomes and MVs (Fig 1 C-E). Interestingly, the sizes of EVs appeared to shift larger when the OSCC cells became transformed to a more metastatic phenotype (Fig 1 C-E). Simultaneously, the metastatic OSCC cells abundantly secreted EVs that contained oncogenic proteins, including EpCAM, EGFR and HSP90 (Fig 2-4). Such an oncogenic signature was more significant in the HSC-3-M3-derived EVs as compared to the HSC-3-EVs. In addition, TRAP1, a mitochondrial HSP, and HSP105 were significantly enriched in the EVs derived from metastatic OSCC cells (Table 1) and expression of these *HSP* genes was correlated with poor prognosis of HNCs (Fig 5, Table 2, Table S3). We hypothesize that EV proteins can reflect metastatic phenotype of cancer cells and thus can be potentially prognostic biomarkers in OSCC cases. We also showed that HSP90α was robustly expressed and secreted by cancer-stem like cells that survive under selective pressure [Eguchi et al., 2018b]. HSP90α level was also elevated in the metastatic OSCC cells and in their EVs (Fig 3, top). This result indicates that HSP90α was robustly expressed in the metastatic OSCC cells and then secreted within

their EVs (Fig 3, top). HSP90β significantly increased in the HSC-3-M3-EVs while intracellular HSP90β was reduced as compared to the parental cells (Fig 3, second from the top), suggesting that HSP90β-EVs can be a novel secretory phenotype of metastatic cancer cells. It has been shown that HSP90 can promote tumor growth and metastasis in breast cancer, leukemia, pancreatic cancer and ovarian cancer [Ciocca and Calderwood, 2005; Ciocca et al., 1993; Neckers and Workman, 2012]. High-level expression of genes encoding HSP90α and HSP90β in clinical tumor samples were also correlated with poor prognosis of HNC cases and with higher stages of HNCs (Fig 5, Table 2). Targeting of HSP90 in cancer chemotherapy is currently a major area of research [Li et al., 2013; Neckers and Workman, 2012]. These chemicals directly target HSP90 proteins, in particular ATP binding and hydrolysis [Trepel et al., 2010] while the HSP90-siRNAs target mRNAs encoding HSP90α and HSP90β individually led to mRNA degradation. The siRNA-mediated double knockdown of HSP90α and HSP90β significantly reduced the survival of metastatic OSCC cells whereas each single knockdown showed lesser effects (Fig 6), suggesting a mutually compensatory system of these HSP90. The HSP90-siRNA could reduce cellular as well as exosomal HSP90 at mRNA and protein levels when administrated to EV-producing cancer cells. Moreover, siRNA species could be carried by EVs that transfer cargos into recipient cells in a similar way to EV transport of microRNA species. The HSP90-contained EVs may sustain survival and metastatic phenotypes of cancer cells in autocrine and paracrine manners. The siRNA-mediated targeting of HSP90 can thus efficiently reduce these phenotypes of cancer cells. In addition, triple knockdown of the HSP90α/β and their co-chaperone CDC37 also significantly lowered survival of the

HSC-3-M3 cells and might be more effective than HSP90 double knockdown (Fig 6C). The mechanism by which chaperone-enriched EVs involve OSCC progression and metastasis is currently undertaken.

One of the interesting findings in the study was that levels of proteins in the EV are not necessarily predicated by their relative intracellular concentrations (Fig. 3). The relative behavior of Hsp90α and Hsp90β was typical in this way. Although intracellular Hsp90α levels appeared relatively lower than those of Hsp90β, secretion of the alpha isoform appeared to be considerably greater (Fig. 3). Indeed the extracellular functions of Hsp90α are of growing significance and mechanisms of secretion involving phosphorylation, ubiquitinylation and upstream activation by HIF1α have been proposed [Li et al., 2007; Sarkar and Zohn, 2012; Wang et al., 2009]. Such mechanisms may serve to enrich individual proteins in EV in a regulated manner.

In addition to these HSPs, the metastatic OSCC-derived larger EVs contained abundant cytoskeletal proteins, particular enzymes and less ECM proteins as compared to the smaller EVs that were secreted by parental cells (Fig 4). It was recently shown that adipocytes also secreted two types of EVs: large EVs that contained molecular chaperones and cytoskeletal proteins and smaller EVs containing ECM proteins [Durcin et al., 2017]. Thus, it may be a general finding that large EVs or MVs are enriched with chaperones and cytoskeletal proteins while small EVs or exosomes can be enriched with ECMs within particular cell types. Metastatic cancer cells may secrete chaperone-enriched enlarged EVs whereas benign tumors may secrete chaperoneless small EVs. We also showed that cancer cells produced intracellular matrix metalloproteinase 3 (MMP3) that can regulate gene

expression of chaperones and matricellular protein CCN2 [Eguchi et al., 2017; Eguchi et al., 2010]. MMPs can regulate production and status of ECM-EVs. Therefore, roles and targeting of MMPs in regulation of EV are currently being undertaken.

In conclusion, metastatic oral cancer cells secrete extracellular vesicles that are enriched with molecular chaperones, including HSP90α and HSP90β. The HSP90, TRAP1, and HSP105 are potentially EV biomarkers of cancer metastatic phenotype as well as prognostic biomarkers in HNCs.

ACKNOWLEDGEMENTS. This paper is dedicated to the memory of one of the coauthors, Professor Ken-ichi Kozaki, who passed away on May 29, 2016. The authors thank Seiji Tamaru, Haruo Urata and Kazuko Kobayashi for helpful operation of LC-MS/MS, TEM and Zetasizer, respectively, and members of dept. of Dental Pharmacology and of dept. of Oral and Craniofacial Surgery at Okayama Univ. for support.

CONFLICTS OF INTEREST. The authors have no competing financial interests to declare.

FUNDING. This work was supported by JSPS KAKENHI, grant numbers JP16K11722 (to JM and TE), JP17K11642 (to TE) and JP17K11669 (to KO, CS, and TE) and a Ryobi Teien Memorial Foundation Grant (to TE). Mitsui Knowledge Industry Co., Ltd. provided support in the form of salaries for JF, but did not have any additional role in the study design, data collection and analysis, decision to publish, or preparation of the manuscript.

REFERENCES

Andreu Z, Yanez-Mo M. 2014. Tetraspanins in extracellular vesicle formation and function. Front Immunol 5:442.

Calderwood SK. 2015. Cdc37 as a co-chaperone to Hsp90. Subcell Biochem 78:103-12.

Calderwood SK. 2018. Heat shock proteins and cancer: intracellular chaperones or extracellular signalling ligands? Philos Trans R Soc Lond B Biol Sci 373.

Ciocca D, Calderwood S. 2005. Heat shock proteins in cancer: diagnostic, prognostic, predictive, and treatment implications. Cell Stress & Chaperones 10:86.

Ciocca D, Clark G, Tandon A, Fuqua S, Welch W, McGuire W. 1993. Heat shock protein hsp70 in patients with axillary lymph node-negative breast cancer: prognostic implications. J Natl Cancer Inst 85:570-4.

Clayton A, Turkes A, Navabi H, Mason MD, Tabi Z. 2005. Induction of heat shock proteins in B-cell exosomes. J Cell Sci 118:3631-8.

Colombo M, Raposo G, Thery C. 2014. Biogenesis, secretion, and intercellular interactions of exosomes and other extracellular vesicles. Annu Rev Cell Dev Biol 30:255-89.

Durcin M, Fleury A, Taillebois E, Hilairet G, Krupova Z, Henry C, Truchet S, Trotzmuller M, Kofeler H, Mabilleau G, Hue O, Andriantsitohaina R, Martin P, Le Lay S. 2017. Characterisation of adipocyte-derived extracellular vesicle subtypes identifies distinct protein and lipid signatures for large and small extracellular vesicles. J Extracell Vesicles 6:1305677.

Eguchi T, Calderwood SK, Takigawa M, Kubota S, Kozaki KI. 2017. Intracellular MMP3 Promotes HSP Gene Expression in Collaboration With Chromobox Proteins. J Cell Biochem 118:43-51.

Eguchi T, Kubota S, Kawata K, Mukudai Y, Uehara J, Ohgawara T, Ibaragi S, Sasaki A, Kuboki T, Takigawa M. 2008. Novel transcription-factor-like function of human matrix metalloproteinase 3 regulating the CTGF/CCN2 gene. Mol Cell Biol 28:2391-413.

Eguchi T, Kubota S, Kawata K., Mukudai Y., Uehara J., Ohgawara T., Ibaragi S, Sasaki A., Kuboki T, Takigawa M. 2010. Novel Transcriptional Regulation of CCN2/CTGF by Nuclear Translocation of MMP3. Dordrecht, Nertherlands: Springer. p 255-264.

Eguchi T, Lang BJ, Murshid A, Prince T, Gong J, Calderwood SK. 2018a. Regulatory roles for Hsp70 in cancer incidence and tumor progression. In Galigniana MD, editor^editors. Frontiers in Structural Biology. Bentham Science, p 1-22.

Eguchi T, Sogawa C, Okusha Y, Uchibe K, Iinuma R, Ono K, Nakano K, Murakami J, Itoh M, Arai K, Fujiwara T, Namba Y, Murata Y, Shimomura M, Okamura H, Takigawa M, Nakatsura T, Kozaki K, Okamoto K, Calderwood S. 2018b. Organoids with Cancer Stem Cell-like Properties Secrete Exosomes and HSP90 in a 3D NanoEnvironment. PLOS ONE 13:e0191109.

Fujita Y, Yoshioka Y, Ochiya T. 2016. Extracellular vesicle transfer of cancer pathogenic components. Cancer Sci 107:385-90.

Gong J, Weng D, Eguchi T, Murshid A, Sherman MY, Song B, Calderwood SK. 2015. Targeting the hsp70 gene delays mammary tumor initiation and inhibits tumor cell metastasis. Oncogene 34:5460-71.

Heijnen H, Schiel A, Fijnheer R, Geuze H, Sixma J. 1999. Activated platelets release two types of membrane vesicles: microvesicles by surface shedding and exosomes derived from exocytosis of multivesicular bodies and alpha-granules. Blood 94:3791-99.

Jemal A, Bray F, Center MM, Ferlay J, Ward E, Forman D. 2011. Global cancer statistics. CA Cancer J Clin 61:69-90.

Kowalski L, Sanabria A. 2007. Elective neck dissection in oral carcinoma: a critical review of the evidence. Acta Otorhinolaryngol Ital 27:113-7.

Li W, Li Y, Guan S, Fan J, Cheng CF, Bright AM, Chinn C, Chen M, Woodley DT. 2007. Extracellular heat shock protein-90alpha: linking hypoxia to skin cell motility and wound healing. EMBO J 26:1221-33.

Li W, Tsen F, Sahu D, Bhatia A, Chen M, Multhoff G, Woodley DT. 2013. Extracellular Hsp90 (eHsp90) as the actual target in clinical trials: intentionally or unintentionally. Int Rev Cell Mol Biol 303:203-35.

Lobb RJ, Becker M, Wen SW, Wong CS, Wiegmans AP, Leimgruber A, Moller A. 2015. Optimized exosome isolation protocol for cell culture supernatant and human plasma. J Extracell Vesicles 4:27031.

Lotvall J, Hill AF, Hochberg F, Buzas EI, Di Vizio D, Gardiner C, Gho YS, Kurochkin IV, Mathivanan S, Quesenberry P, Sahoo S, Tahara H, Wauben MH, Witwer KW, Thery C. 2014. Minimal experimental requirements for definition of extracellular vesicles and their functions: a position statement from the

International Society for Extracellular Vesicles. J Extracell Vesicles 3:26913.

Madhavan B, Yue S, Galli U, Rana S, Gross W, Muller M, Giese NA, Kalthoff H, Becker T, Buchler MW, Zoller M. 2015. Combined evaluation of a panel of protein and miRNA serum-exosome biomarkers for pancreatic cancer diagnosis increases sensitivity and specificity. Int J Cancer 136:2616-27.

Mathivanan S, Fahner CJ, Reid GE, Simpson RJ. 2012. ExoCarta 2012: database of exosomal proteins, RNA and lipids. Nucleic Acids Res 40:D1241-4.

Mathivanan S, Simpson RJ. 2009. ExoCarta: A compendium of exosomal proteins and RNA. Proteomics 9:4997-5000.

Matsui T, Ota T, Ueda Y, Tanino M, Odashima S. 1988. Isolation of a highly metastatic cell line to lymph node in human oral squamous cell carcinoma by orthotopic implantation in nude mice. Oral Oncology 34:253-256.

Munz M, Baeuerle PA, Gires O. 2009. The emerging role of EpCAM in cancer and stem cell signaling. Cancer Res 69:5627-9.

Murshid A, Eguchi T, Calderwood SK. 2013. Stress proteins in aging and life span. Int J Hyperthermia 29:442-7.

Nakai W, Yoshida T, Diez D, Miyatake Y, Nishibu T, Imawaka N, Naruse K, Sadamura Y, Hanayama R. 2016. A novel affinity-based method for the isolation of highly purified extracellular vesicles. Sci Rep 6:33935.

Neckers L, Workman P. 2012. Hsp90 molecular chaperone inhibitors: are we there yet? Clin Cancer Res 18:64-76.

Neveille B, Day T. 2002. Oral cancer and precancerous lesions. CA Cancer J Clin 52:195-215.

Ono M, Kamita M, Murakoshi Y, Matsubara J, Honda K, Miho B, Sakuma T, Yamada T. 2012. Biomarker Discovery of Pancreatic and Gastrointestinal Cancer by 2DICAL: 2-Dimensional Image-Converted Analysis of Liquid Chromatography and Mass Spectrometry. Int J Proteomics 2012:897412.

Overmiller AM, Pierluissi JA, Wermuth PJ, Sauma S, Martinez-Outschoorn U, Tuluc M, Luginbuhl A, Curry J, Harshyne LA, Wahl JK, 3rd, South AP, Mahoney MG. 2017. Desmoglein 2 modulates

extracellular vesicle release from squamous cell carcinoma keratinocytes. Faseb j 31:3412-3424.

Pan BT, Teng K, Wu C, Adam M, Johnstone RM. 1985. Electron microscopic evidence for externalization of the transferrin receptor in vesicular form in sheep reticulocytes. J Cell Biol 101:942-8.

Raposo G, Stoorvogel W. 2013. Extracellular vesicles: exosomes, microvesicles, and friends. J Cell Biol 200:373-83.

Sano D, Myers JN. 2007. Metastasis of squamous cell carcinoma of the oral tongue. Cancer Metastasis Rev 26:645-62.

Sarkar AA, Zohn IE. 2012. Hectd1 regulates intracellular localization and secretion of Hsp90 to control cellular behavior of the cranial mesenchyme. J Cell Biol 196:789-800.

Shapiro IM, Landis WJ, Risbud MV. 2015. Matrix vesicles: Are they anchored exosomes? Bone 79:29-36.

Skog J, Wurdinger T, van Rijn S, Meijer DH, Gainche L, Sena-Esteves M, Curry WT, Jr., Carter BS, Krichevsky AM, Breakefield XO. 2008. Glioblastoma microvesicles transport RNA and proteins that promote tumour growth and provide diagnostic biomarkers. Nat Cell Biol 10:1470-6.

Stivarou T, Patsavoudi E. 2015. Extracellular molecules involved in cancer cell invasion. Cancers (Basel) 7:238-65.

Trepel J, Mollapour M, Giaccone G, Neckers L. 2010. Targeting the dynamic HSP90 complex in cancer. Nat Rev Cancer 10:537-49.

Uhlen M, Fagerberg L, Hallstrom BM, Lindskog C, Oksvold P, Mardinoglu A, Sivertsson A, Kampf C, Sjostedt E, Asplund A, Olsson I, Edlund K, Lundberg E, Navani S, Szigyarto CA, Odeberg J, Djureinovic D, Takanen JO, Hober S, Alm T, Edqvist PH, Berling H, Tegel H, Mulder J, Rockberg J, Nilsson P, Schwenk JM, Hamsten M, von Feilitzen K, Forsberg M, Persson L, Johansson F, Zwahlen M, von Heijne G, Nielsen J, Ponten F. 2015. Proteomics. Tissue-based map of the human proteome. Science 347:1260419.

Valadi H, Ekstrom K, Bossios A, Sjostrand M, Lee JJ, Lotvall JO. 2007. Exosome-mediated transfer of mRNAs and microRNAs is a novel mechanism of genetic exchange between cells. Nat Cell Biol 9:654-9.

Wang X, Song X, Zhuo W, Fu Y, Shi H, Liang Y, Tong M, Chang G, Luo Y. 2009. The regulatory mechanism of Hsp90alpha secretion and its function in tumor malignancy. Proc Natl Acad Sci U S A

106:21288-93.

Witwer KW, Buzas EI, Bemis LT, Bora A, Lasser C, Lotvall J, Nolte-'t Hoen EN, Piper MG, Sivaraman S, Skog J, Thery C, Wauben MH, Hochberg F. 2013. Standardization of sample collection, isolation and analysis methods in extracellular vesicle research. J Extracell Vesicles 2.

Workman P, Burrows F, Neckers L, Rosen N. 2007. Drugging the cancer chaperone HSP90: combinatorial therapeutic exploitation of oncogene addiction and tumor stress. Ann N Y Acad Sci 1113:202-16.

Yoshioka Y, Kosaka N, Konishi Y, Ohta H, Okamoto H, Sonoda H, Nonaka R, Yamamoto H, Ishii H, Mori M, Furuta K, Nakajima T, Hayashi H, Sugisaki H, Higashimoto H, Kato T, Takeshita F, Ochiya T. 2014. Ultra-sensitive liquid biopsy of circulating extracellular vesicles using ExoScreen. Nat Commun 5:3591.

FIGURE LEGENDS

Fig 1. EVs secreted by the metastatic oral cancer cells were larger than those secreted by the parental cells. (A, B) Representative TEM images of EVs secreted from the parental HSC-3 (A) and the metastatic HSC-3-M3 cells (B). Arrowheads indicate EVs with cup-shaped morphology. Scale bars, 200 nm. (C) Combined box-and-whisker and dot plots of EVs. Major axes of EVs were measured in TEM images. n = 50. *P = 0.045 (paired *t*-test). (D, E) Particle diameter distribution analysis of EVs secreted by (D) and HSC-3-M3 cells (E).

Fig 2. Metastatic OSCC cells secrete EpCAM-enriched EVs including exosomes more than the parental cells. Cells were cultured for 2 days in serum-free medium from which EV fractions were prepared. (A) Western blot showing EpCAM and CD9. EV fractions were prepared from HSC-3 and HSC-3-M3 cells using the polymer-based precipitation or

ultracentrifugation methods. Equal amounts of EV proteins were loaded into each lane. Representative data are shown. (B-E) The concentration of CD9 positive exosomes (B, C) or CD9-EpCAM double positive exosomes (D, E) v/w % per EV fraction (B, D) or secreted amount (ng) per 10^6 cells (C, E) were quantified by using ExoScreen.

Fig 3. HSP90 and EpCAM increased in EVs released by lymph-node-metastatic OSCC cells. The EV and cellular fractions were prepared at the same time point after 2 days of serum-deprivation. Equal amounts of EV- or cellular proteins were used for each Western blotting analysis. HSP90α, HSP90β, EpCAM, EGFR, GAPDH and β-actin in the EVs and whole cell lysates were analyzed. M.W., molecular weight.

Fig 4. EV proteomics and chaperonomics of OSCC cells. (A) Venn diagram comparing proteins in OSCC-EVs with proteins in ExoCarta database. Total 192 types of proteins were detected in EVs by the proteomics. ExoCarta database documented 6,514 proteins. Among the 192 protein species, 108 protein species (56.3%) found in the OSCC-derived EVs were already documented in the ExoCarta database, whereas 84 protein species (43.7%) were novel EV proteins. (B) Venn diagram comparing differential EV proteome signatures of HSC-3 and HSC-3-M3. Among top 50 EV protein species found in each cell line 34 protein species (68%) were common between the two EV fractions, whereas the remaining 16 protein species (32%) were distinctive in each OSCC-EV fraction. (C, D) Functional properties of EV proteomes of the parental and the metastatic OSCC cells. Top 16 protein species in each EV fraction derived from HSC-3 and HSC-3-M3 were functionally

categorized, and numbers of protein species (C) and total MS scores (D) were distributed to each category. Molecular chaperones were found in HSC-3-M3-EV with high scores as compared to HSC-3-EVs. (E) Venn diagram comparing differential EV chaperones signatures of HSC-3 and HSC-3-M3. Among 14 EV chaperone species found in each cell line 9 chaperones species (64%) were highly detected in HSC-3-M3, whereas only 1 chaperone specie (7%) was highly detected in HSC-3.

Fig. 5. Prognostic values of HSPs in HNC cases. Kaplan-Meier survival analysis for HSP90AA1 (A), HSP90AB1 (B), TRAP1 (C) and HSPH1 (D) genes in HNCs were retrieved from The Human Protein Atlas. Expression values of each gene were divided into high (purple line) and low (blue line) expression using each best cut off value as the threshold value. P values correspond to the log-rank test comparing the survival curves.

Fig 6. Targeting of HSP90 in metastatic OSCC cells. HSC-3-M3 cells were transfected with chaperone-targeting siRNA (siHSP90α, siHSP90β or siCDC37) or non-targeting dsRNA (siCtrl). (A) Western blot showing single, double and triple knockdown of HSP90α, HSP90β and CDC37 in HSC-3-M3 cells. Equal amounts of cellular proteins were used for each lane. (B) Survival of the HSC-3-M3 cells upon chaperone knockdown. Numbers of adherent cells 3 days after transfection of siRNA were shown. n = 3. *P < 0.05, **P < 0.01 (paired *t*-test). (C) Representative photomicrographs of the cells at day 3 after transfection of siRNA. Scale bar, 100 μm.

Fig S1. Polymer-based precipitation method and ultracentrifugation method for preparation of EVs. (A) A workflow of the EV preparation methods. (B) Transmission electron microscopy of EVs prepared by using the PBP method (upper images) and the UC method (lower images). Scale bars, 200 nm. (C) Ratio of EV protein concentration per cellular protein concentration.

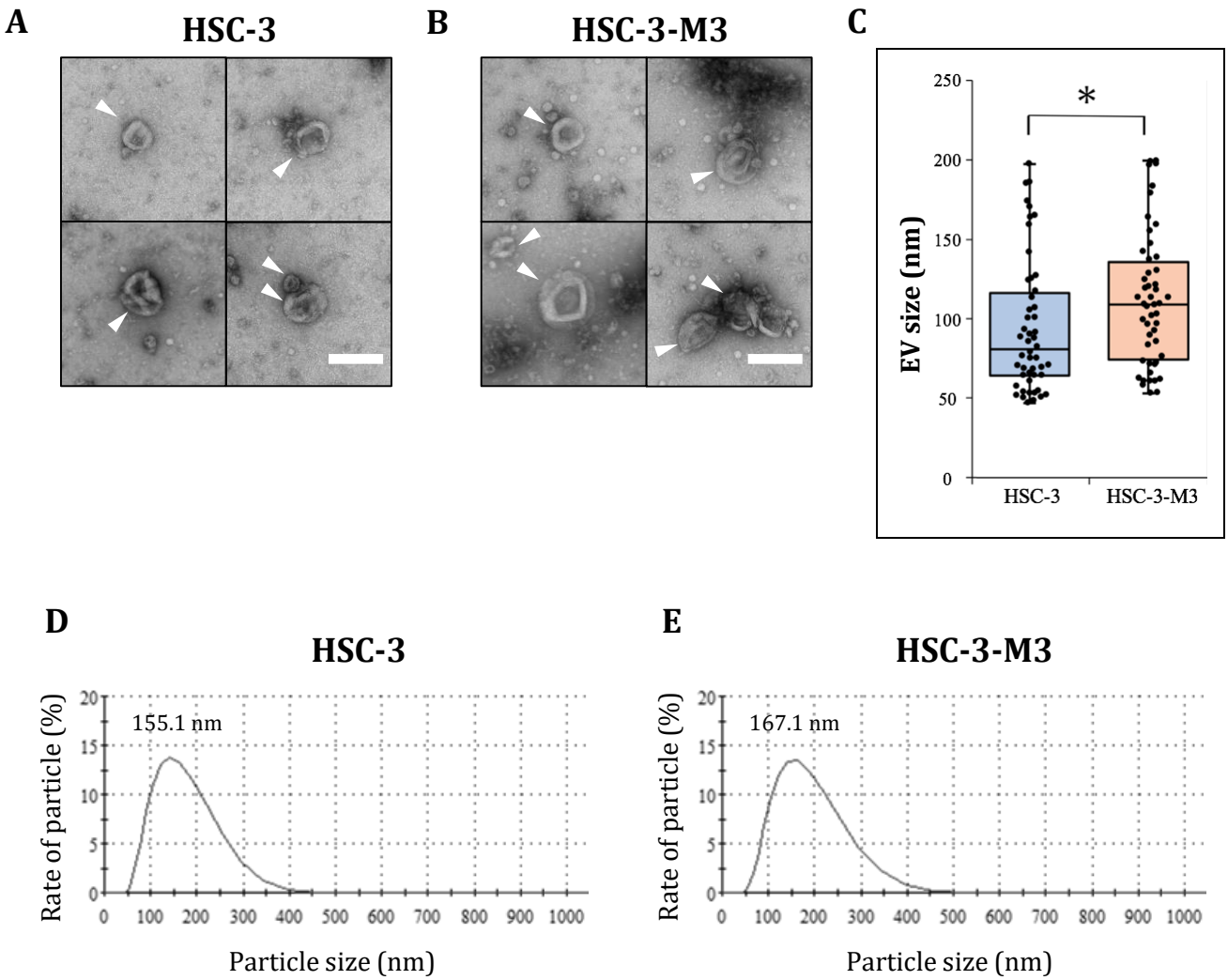
A
HSC-3
B
HSC-3-M3
C
EV size (nm)
250
200
150
100
50
0
*
HSC-3
HSC-3-M3
D
HSC-3
155.1 nm
Rate of particle (%)
Particle size (nm)
E
HSC-3-M3
167.1 nm
Rate of particle (%)
Particle size (nm)

Fig. 1

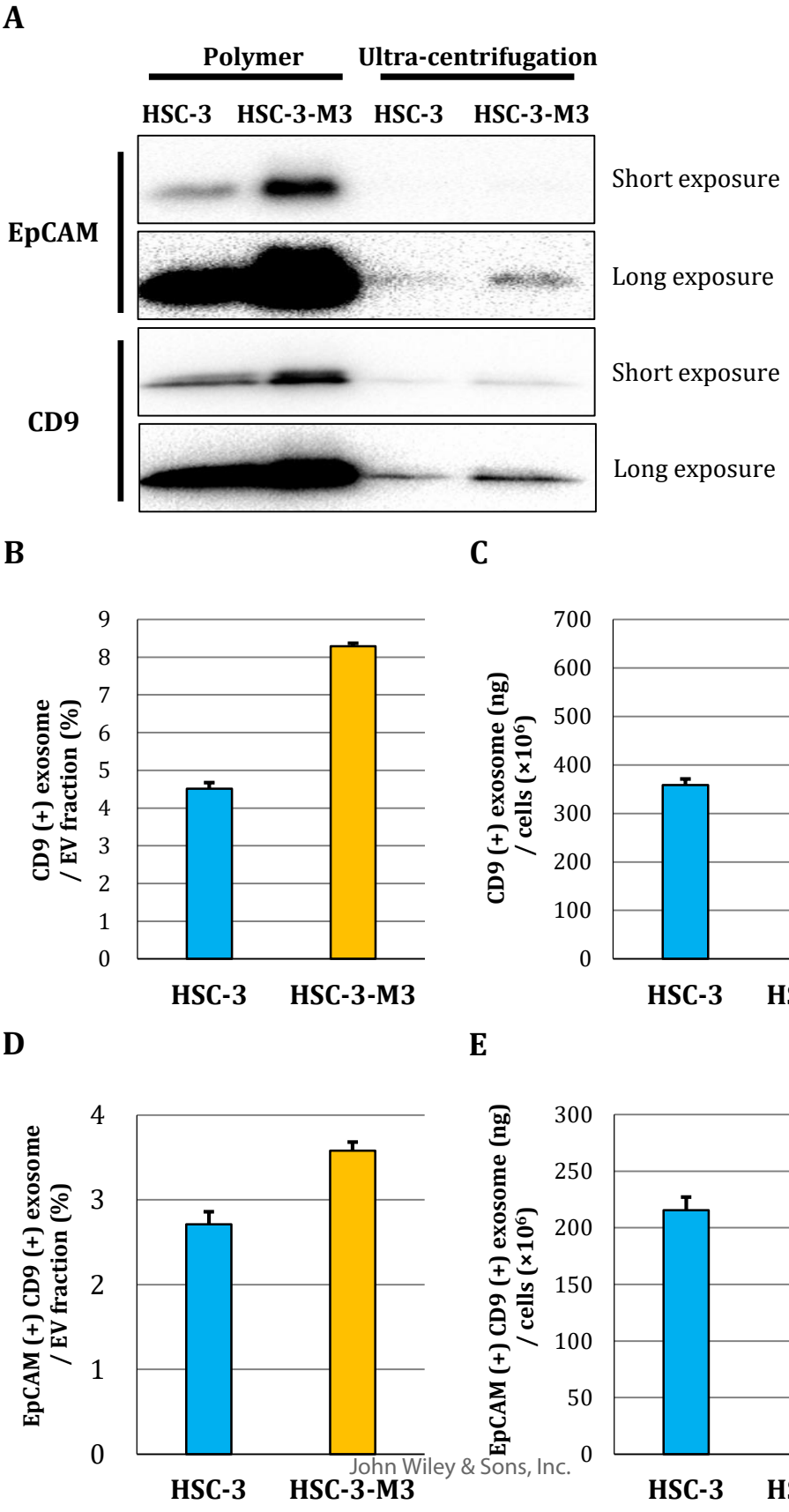

Fig. 2

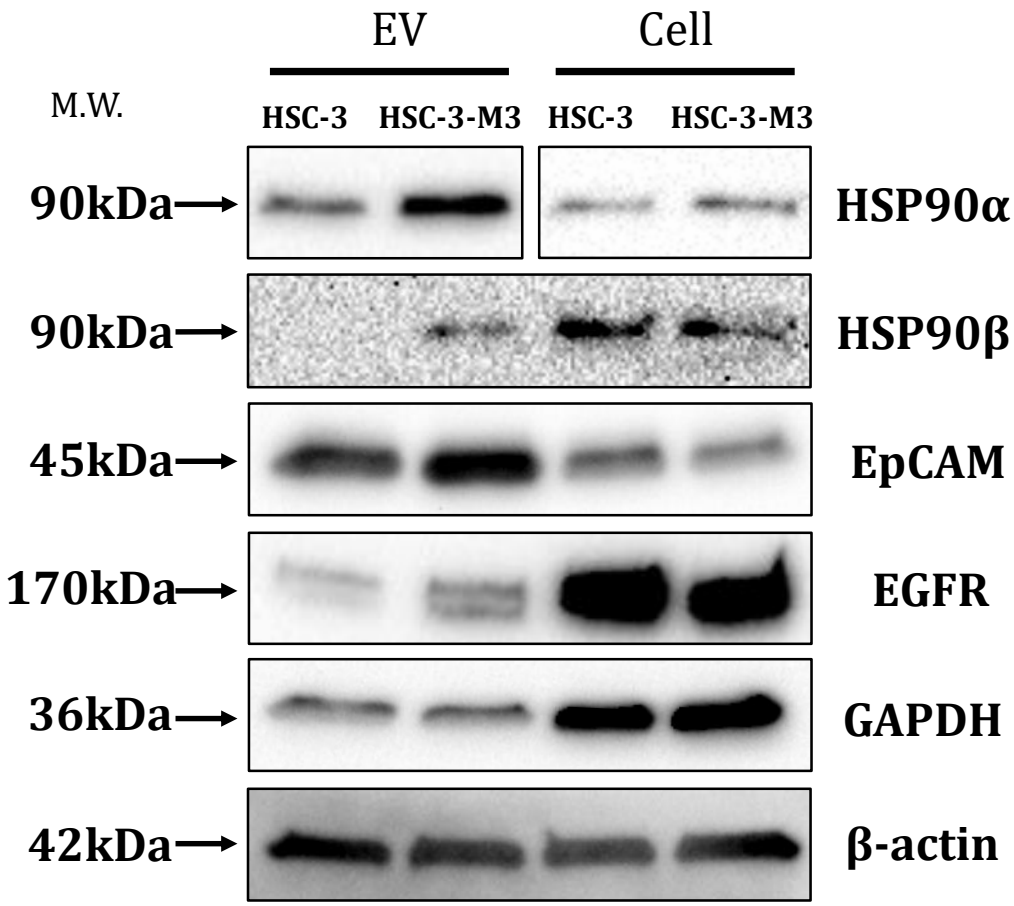
EV
Cell
M.W.
HSC-3
HSC-3-M3
HSC-3
HSC-3-M3
90kDa
HSP90α
90kDa
HSP90β
45kDa
EpCAM
170kDa
EGFR
36kDa
GAPDH
42kDa
β-actin

Fig. 3

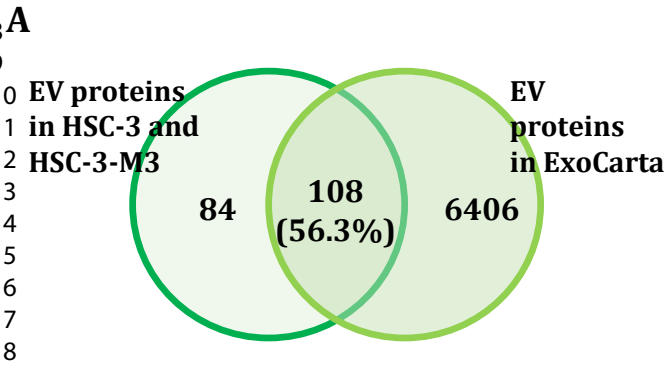
A
EV proteins in HSC-3 and HSC-3-M3
84
108 (56.3%)
EV proteins in ExoCarta
6406

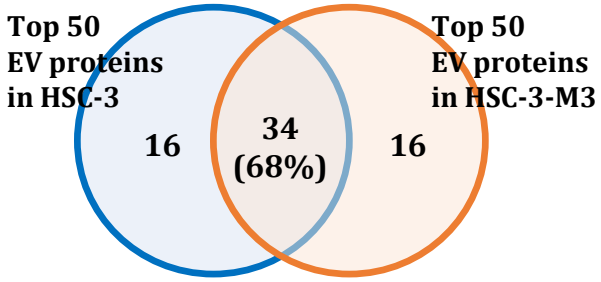
B
Top 50 EV proteins in HSC-3
16
34 (68%)
Top 50 EV proteins in HSC-3-M3
16

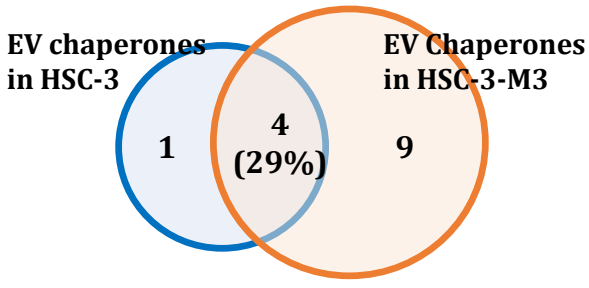
E
EV chaperones in HSC-3
1
4 (29%)
EV Chaperones in HSC-3-M3
9

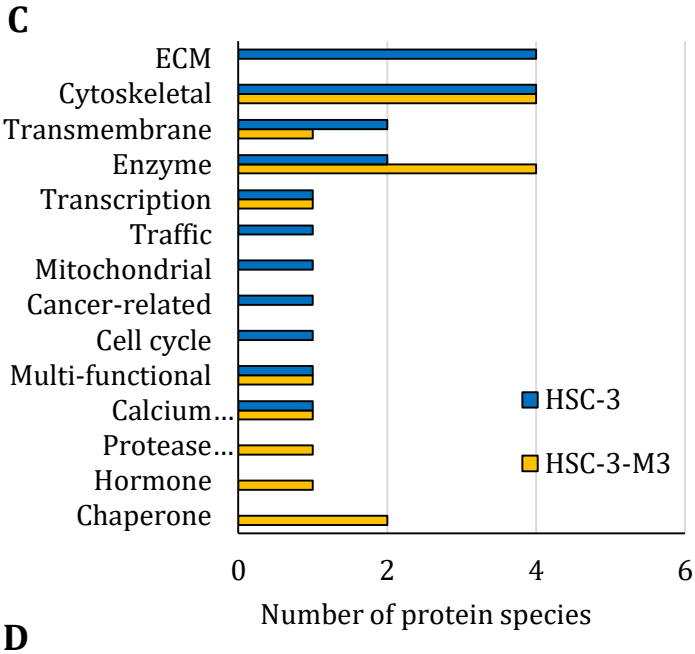
C
ECM
Cytoskeletal
Transmembrane
Enzyme
Transcription
Traffic
Mitochondrial
Cancer-related
Cell cycle
Multi-functional
Calcium...
Protease...
Hormone
Chaperone
HSC-3
HSC-3-M3
0
2
4
6
Number of protein species

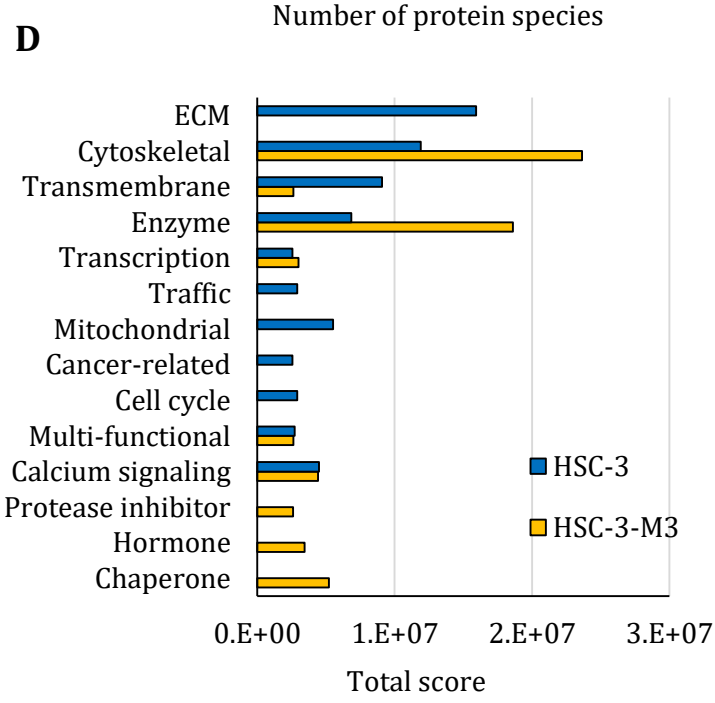
D
ECM
Cytoskeletal
Transmembrane
Enzyme
Transcription
Traffic
Mitochondrial
Cancer-related
Cell cycle
Multi-functional
Calcium signaling
Protease inhibitor
Hormone
Chaperone
HSC-3
HSC-3-M3
0.E+00
1.E+07
2.E+07
3.E+07
Total score

Fig. 4

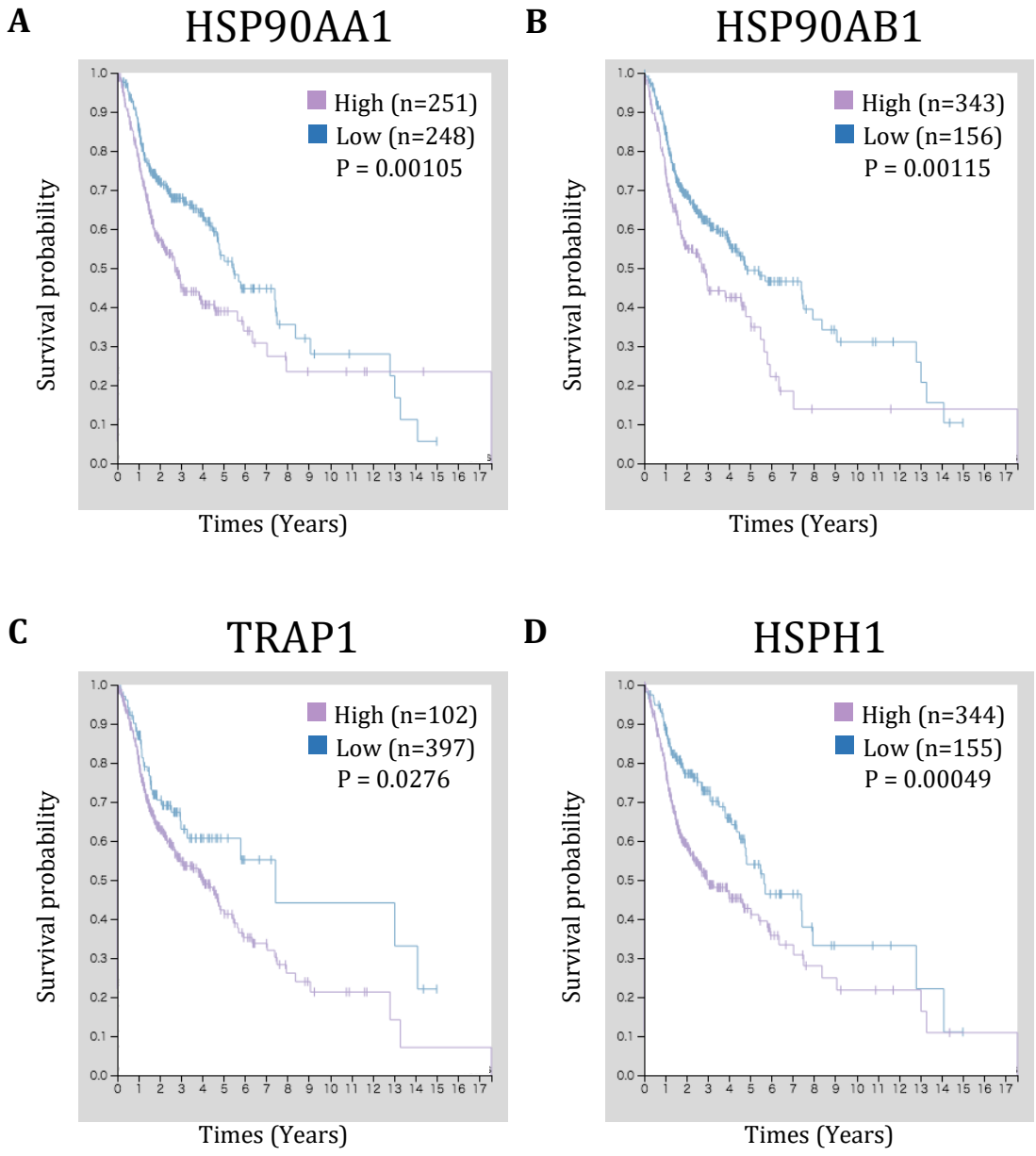
A
HSP90AA1
High (n=251)
Low (n=248)
P = 0.00105
Survival probability
Times (Years)
B
HSP90AB1
High (n=343)
Low (n=156)
P = 0.00115
Survival probability
Times (Years)
C
TRAP1
High (n=102)
Low (n=397)
P = 0.0276
Survival probability
Times (Years)
D
HSPH1
High (n=344)
Low (n=155)
P = 0.00049
Survival probability
Times (Years)

Fig. 5

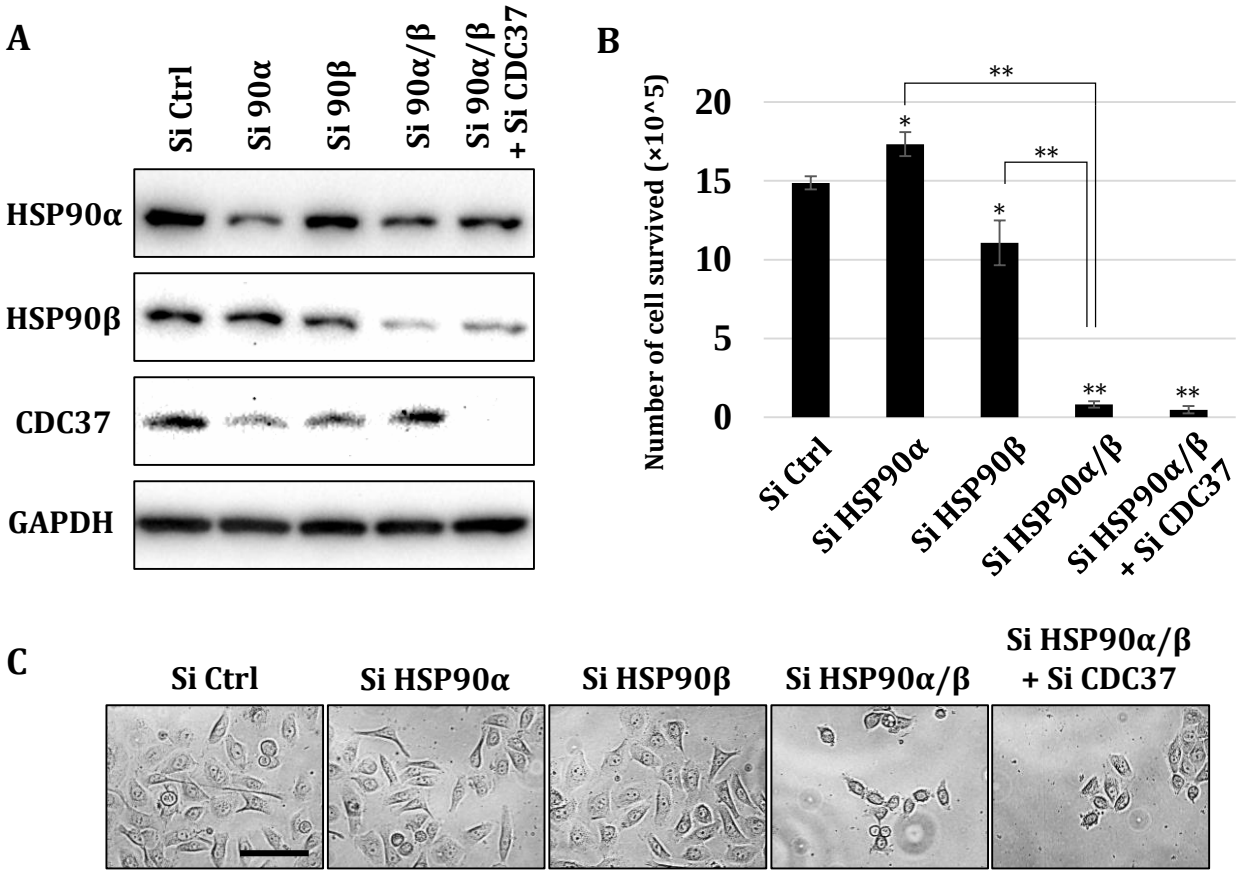
A
Si Ctrl
Si 90α
Si 90β
Si 90α/β
Si 90α/β + Si CDC37
HSP90α
HSP90β
CDC37
GAPDH
B
Number of cell survived (×10^5)
20
15
10
5
0
**
*
**
*
**
**
Si Ctrl
Si HSP90α
Si HSP90β
Si HSP90α/β
Si HSP90α/β + Si CDC37
C
Si Ctrl
Si HSP90α
Si HSP90β
Si HSP90α/β
Si HSP90α/β + Si CDC37

Fig. 6

Table 1. List of molecular chaperones detected in OSCC-EVs.

Chaperones	MS score ratio (HSC-3-M3/HSC-3)	Note
TRAP1 / HSP75	2.95	Heat shock protein 75 kDa, mitochondrial
HSP90AB1 / HSP90β	2.23	Heat shock protein HSP 90-beta
HSP90AA1 / HSP90α	1.78	Heat shock protein HSP 90-alpha
HSPH1 / HSP105	1.78	Heat shock protein 105 kDa
HSPA1A / HSP72	1.7	Heat shock 70 kDa protein 1A
CCT8	1.5	T-complex protein 1 subunit theta
CCT6A	1.29	T-complex protein 1 subunit zeta
HSPA6 / HSP70B'	1.23	Heat shock 70 kDa protein 6
HSPA8 / HSC70	1.23	Heat shock cognate 71 kDa protein
CCT5	1.12	T-complex protein 1 subunit epsilon
CCT2	1.07	T-complex protein 1 subunit beta
TCP1	0.92	T-complex protein 1 subunit alpha
HSPA5 / GRP78	0.85	78 kDa glucose-regulated protein
CCT4	0.67	T-complex protein 1 subunit delta

Table 2. Correlation between HNC stages and HSP expression levels in the tumors.

	HSP90AA1	HSP90AB1	TRAP1	HSPH1
Stage	**Ratio (High / Low)**	**Ratio (High / Low)**	**Ratio (High / Low)**	**Ratio (High / Low)**
Ⅰ	0.39 (7 / 18)	0.14 (3 / 22)	2.57 (18 / 7)	3.17 (19 / 6)
Ⅱ	1.03 (35 / 34)	0.47 (22 / 47)	4.91 (54 / 11)	2.29 (48 / 21)
Ⅲ	0.95 (38 / 40)	0.42 (23 / 55)	4.57 (64 / 14)	2.39 (55 / 23)
Ⅳ	1.21 (142/117)	0.57 (94 / 165)	4.18 (209 / 50)	2.20 (178 / 81)
N/A	0.74 (29 / 39)	0.26 (14 / 54)	3.25 (52 / 16)	1.83 (44 / 24)
Total (n=499)	1.01 (251 / 248)	0.45 (156 / 343)	4.05 (397 / 98)	2.22 (344 / 155)

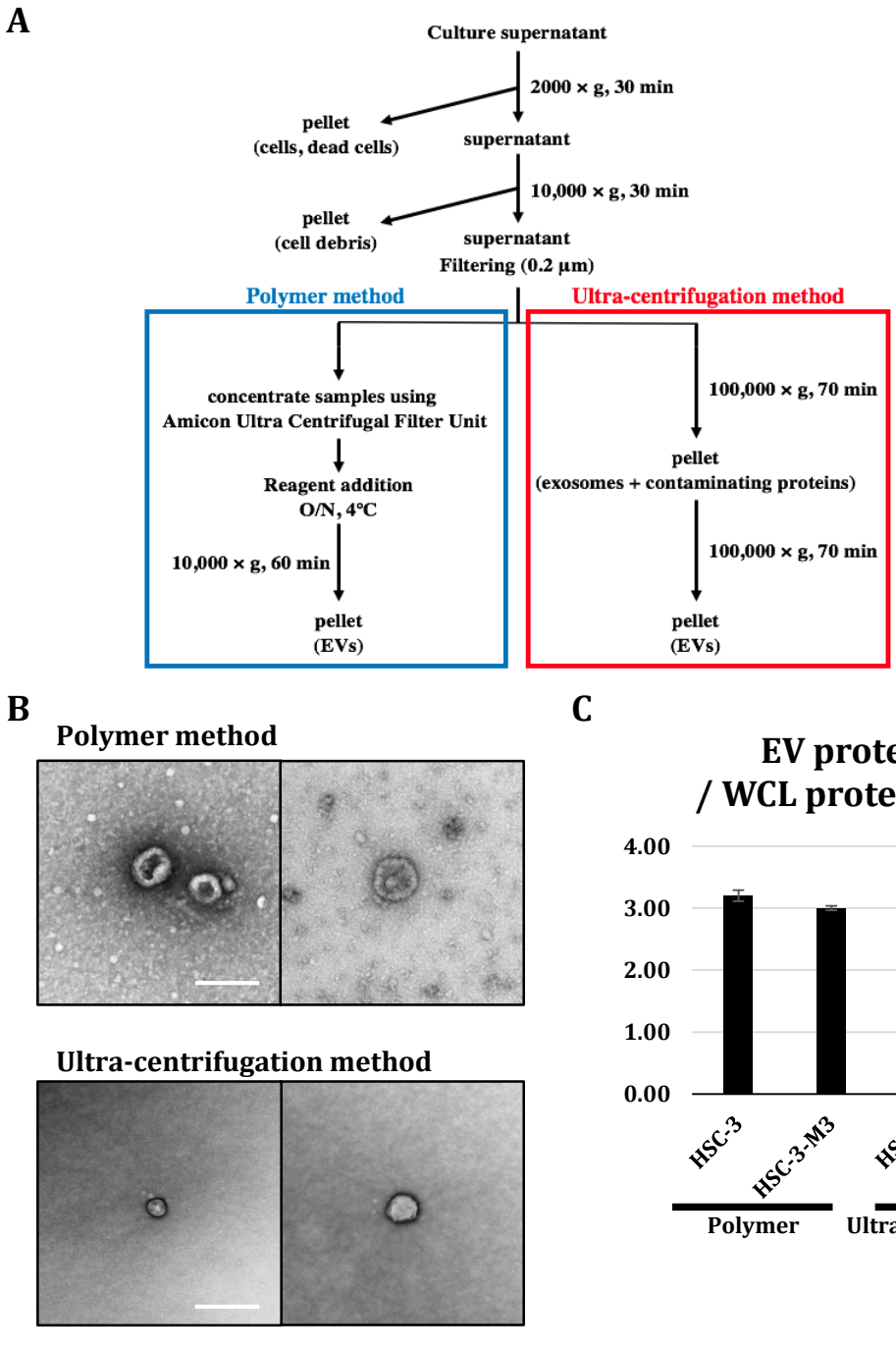
A
Culture supernatant
2000 × g, 30 min
pellet
(cells, dead cells)
supernatant
10,000 × g, 30 min
pellet
(cell debris)
supernatant
Filtering (0.2 μm)
Polymer method
Ultra-centrifugation method
concentrate samples using
Amicon Ultra Centrifugal Filter Unit
Reagent addition
O/N, 4°C
10,000 × g, 60 min
pellet
(EVs)
100,000 × g, 70 min
pellet
(exosomes + contaminating proteins)
100,000 × g, 70 min
pellet
(EVs)
B
Polymer method
Ultra-centrifugation method
C
EV protein
/ WCL protein (%)
4.00
3.00
2.00
1.00
0.00
HSC-3
HSC-3-M3
HSC-3
HSC-3-M3
Polymer
Ultra-centrifugation

Fig. S1

Table S1. A list of siRNAs that target HSP90α, HSP90β, and CDC37 individually.

Name of siRNA	Note	Core sequence of sense (5' to 3')
siHSP90AA#1	hHSP90AA1.NM5348-415	gcugcauauuaaccuuaua
siHSP90AA#2	hHSP90AA1.NM5348-2010	caaacauggagagaaucau
siHSP90AB#1	hHSP90AB1-NM_001271971.1-1353	cagaagacaaggagaauua
siHSP90AB#2	hHSP90AB1-NM_001271971.1-1754	gaagagagcaaggcaaagu
siCDC37#1	hCDC37.NM7065-433	gcaagaaggagaagagcau
siCDC37#2	hCDC37.NM7065-584	gaaacagaucaagcacuuu

Table S2. Comparison of three analysis methods in terms of ratio of EV marker levels.

	Western blotting	LC-MS/MS	ExoScreen
HSP90α	2.04	1.78	NA
HSP90β	1.52	2.23	NA
EpCAM	1.27	UDL	1.25
EGFR	2.18	UDL	NA
CD9	1.03	UDL	1.78
GAPDH	0.96	0.91	NA
β-actin	0.92	0.91	NA

Ratios of scores (HSC-3-M3 / HSC-3) in each analytical method were shown. NA, not applicable. UDL, under detection limit.

Table S3. Correlation between 5-year survival rate and HSP expression levels in HNC patients.

	HSP90AA1	HSP90AB1	TRAP1	HSPH1
Expression cut off	227.1 FPKM	552.0 FPKM	9.4 FPKM	17.6 FPKM
5-year survival low	52%	49%	61%	54%
5-year survival high	39%	35%	41%	41%
Log-rank P value	0.00105	0.00115	0.0276	0.00049

FPKM, Fragments Per Kilobase of exon per Million mapped fragments.